

1 **Chronology and phenomenology of the 1982 and 2015 Wolf volcano eruptions, Galápagos**
2 **Archipelago**

3 Benjamin Bernard^{1*}, Michael J. Stock², Diego Coppola³, Silvana Hidalgo¹, Marco Bagnardi^{4,5},
4 Sally Gibson², Stephen Hernandez¹, Patricio Ramón¹, Matthew Gleeson²

5 ¹ Instituto Geofísico – Escuela Politécnica Nacional, Ladrón de Guevara E11-253 y Andalucía,
6 Quito, Ecuador

7 ² Department of Earth Sciences, University of Cambridge, Cambridge, CB2 3EQ, United Kingdom

8 ³ Dipartimento di Scienze della Terra – Università degli Studi di Torino, Via Valperga Caluso 35,
9 10125 – Torino, Italy

10 ⁴ COMET, School of Earth and Environment, University of Leeds, Leeds, United Kingdom

11 ⁵ Now at Jet Propulsion Laboratory, California Institute of Technology, Pasadena, CA, United States

12
13 **Abstract**

14 The 1982 and 2015 eruptions are the first at Wolf volcano, Galápagos Archipelago, with eyewitness
15 accounts and satellite imagery. Both eruptions are characterized by a rapid, intense initial phase and
16 multiple eruptive vents leading to the formation of large ‘a‘ā lava fields with scarce pāhoehoe
17 deposits, mostly associated with the waning phases. The 1982 eruption started on 28 August from
18 an intra-caldera vent that produced high lava fountaining, but also occurred from a radial fissure on
19 the SE flank. This eruption lasted for at least 9 days and generated approximately 70E+6 m³ of lava.
20 The 2015 eruption started on 25 May from a circumferential fissure that also produced high lava
21 fountaining and deposited reticulite scoria on the flanks of the volcano. For the first time since
22 monitoring Galápagos eruptions, we observed cryptotephra from the 2015 eruption reaching and
23 depositing in mainland Ecuador, 1400 km away from the source. Lava from the 2015
24 circumferential vents covered large areas on the SE and E flanks. On 13 June 2015 the eruption
25 switched to an intra-caldera vent that was active until 30 June, which produced lava flows that
26 covered most of the caldera floor. This eruption lasted 36 days and produced ~116E+6 m³ of lava,
27 making it one of the largest eruptions in the Galápagos since the eruption of Sierra Negra in 1979.
28 The combination of ground-based geophysical surveillance, remote sensing, eyewitness accounts,
29 and detailed field work allows us, for the first time, to constrain the eruptive dynamics of this
30 remote volcano with a day-by-day time resolution. In particular, our approach allows quantification
31 of eruption rates, which represents critical information for understanding volcanic systems and for
32 hazard assessment. First order rheological calculations further enable us to constrain the eruption
33 dynamics and emplacement of the lava fields.

34

35 **Keywords**

36 Wolf volcano; eruptive chronology; lava fountaining; lava flows; eruption rate; reticulite;
37 cryptotephra

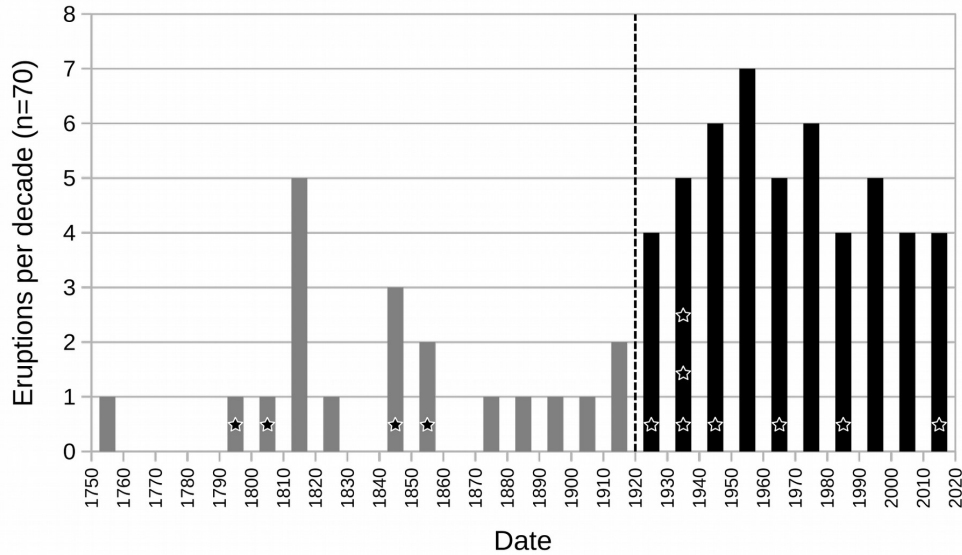
38

39 **1. Introduction**

40 The Galápagos Archipelago (eastern Pacific Ocean) is one of the most active regions of hotspot-
41 related volcanism in the world, along with Hawai'i (north Pacific Ocean) and La Réunion (west
42 Indian Ocean; Simkin, 1984). The earliest reports of eruptive activity in the Galápagos date back to
43 the 18th century but a semi-complete record is only available for the last 100 years, due to the major
44 colonization of the Archipelago at the end of the 19th century and beginning of the 20th century
45 (González et al., 2008; Fig. 1). During this period, the Galápagos Archipelago has experienced, on
46 average, one eruption every two years.

47 Wolf (0.02°N, 91.35°W) is the northernmost volcano on Isabela Island (Fig. 2a), which is formed
48 by the coalescence of four other active volcanoes (Cerro Azul, Sierra Negra, Alcedo, Darwin) and a
49 fifth potentially active volcano (Ecuador). Wolf is a 1705 m-high shield volcano and has
50 experienced 8 eruptions within the last 100 years, equivalent to Sierra Negra. Only Fernandina and
51 Cerro Azul in Galápagos have had more eruptions over the last century, with 20 and 10 eruptive
52 events, respectively. All of the Wolf lava flows that have been analyzed geochemically comprise
53 compositionally-homogeneous basalt, with highly-depleted isotopic compositions similar to typical
54 N-MORBs (Geist et al., 2005). Due to its remote location (110 km from the nearest town) and
55 relatively low eruptive frequency since 1950, little is known about historical activity of Wolf (Geist
56 et al., 2005). However, eyewitness accounts and satellite imagery exist for the two most recent
57 eruptions in 1982 and 2015; these have the potential to provide significant constraints on the
58 eruptive dynamics. This paper aims to present an extensive description of these eruptions by
59 coupling eyewitness accounts, available geophysical data (ground-based and remote sensing), and
60 analyses of eruptive deposits. We use satellite-borne optical, infrared and radar imagery,
61 photogrammetric data from Unmanned Aerial Vehicle (UAV) surveys, and field measurements to
62 map the lava fields and estimate the volume of subaerial products. Characteristics and morphology
63 of the deposits are used to provide first order constraints on the lava rheology. To broaden our
64 understanding of Galápagos volcanic systems, we compare the inferred eruptive dynamics and the
65 evolution of the 1982 and 2015 eruptions at Wolf with accounts of recent eruptions elsewhere in the
66 Galápagos Archipelago.

67

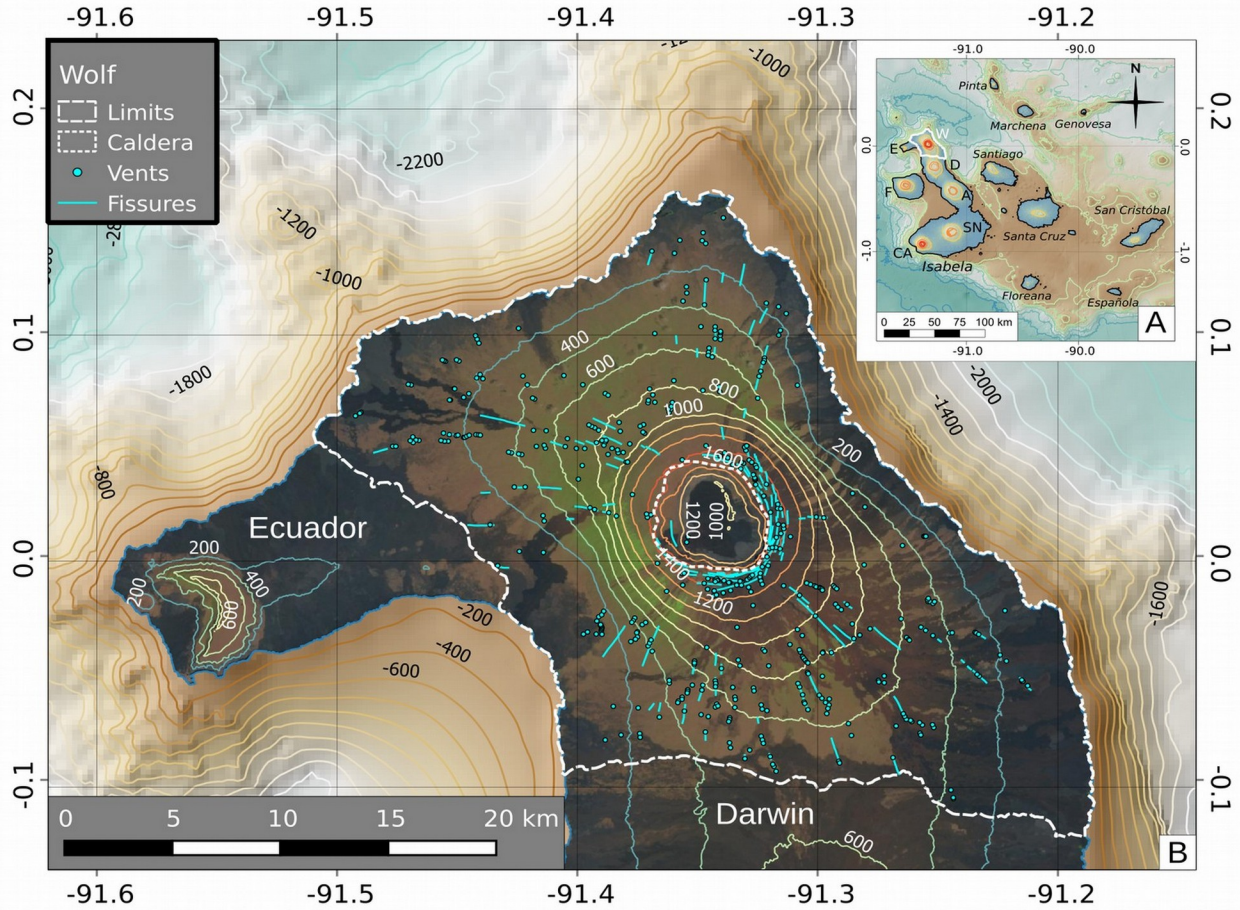


69 Figure 1. Eruptive frequency in the Galápagos Archipelago since 1750 (sources: modified from
 70 Global Volcanism Program, 2013). The gray series corresponds to the pre-1920 incomplete
 71 historical record (~ 1.2 eruptions/decade). The black series corresponds to the post-1920 historical
 72 record, which is considered to be relatively complete (5 eruptions/decade). The black stars with
 73 white outlines are Wolf volcano eruptions.

74 2. Wolf volcano

75 2.1. Morphology

76 Wolf is a large shield volcano with an inverted soup-bowl morphology characterized by gentle
 77 slopes on the lower flank and steep slopes on the upper flank, typical of other volcanoes in the
 78 western Galápagos Archipelago (Simkin and Howard, 1970). It has a rhomboidal shape (41×21 km)
 79 elongated in the NW-SE direction, and is bordered by Ecuador volcano to the west and Darwin
 80 volcano to the south (Fig. 2). The eastern, northern and south-western sides of Wolf volcano steeply
 81 dip towards the Pacific Ocean floor to a depth of ~3 km below sea level. The subaerial edifice of
 82 Wolf covers ~600 km² and has a volume of ~280 km³ (Bernard and Andrade, in review). It is
 83 classified as a Type 2 Galápagos shield volcano, along with Cerro Azul and Fernandina; these have
 84 distinctly steeper slopes at intermediate elevations and deeper calderas than Type 1 volcanoes such
 85 as Sierra Negra, Alcedo and Darwin (Mouginis-Mark et al., 1996). The summit caldera is slightly
 86 elongated in the NW-SE direction (Munro and Rowland, 1996) and has an area of ~25 km² and a
 87 volume of ~10 km³ (6.2×5.3 km-diameter, 700 m-deep; Bernard and Andrade, in review). The
 88 caldera hosts several benches with the largest one (3.9×0.9 km) located on the western side, ~260 m
 89 below the caldera rim. The caldera walls also exhibit landslide scars, with an associated debris
 90 avalanche deposit covering the south-east part of the caldera floor. The south-west side of the
 91 caldera is the site of two eruptive vents that were active during most of the 1982 eruption (Geist et
 92 al., 2005).



94 Figure 2. A) Location of Wolf volcano (W) and Isabela Island in the Galápagos Archipelago (A:
 95 Alcedo; CA: Cerro Azul, D: Darwin, E: Ecuador; F: Fernandina; SN: Sierra Negra); B) fissures and
 96 vents locations on Wolf volcano (modified from Bernard and Andrade, in review). Bathymetry: 250
 97 m global multi-resolution topography, Ryan et al. (2009); Islands topography: JAXA 30 m digital
 98 elevation model; satellite image: Landsat 7, acquired in 2001.

99

100 2.2. Structures

101 The shape of Wolf volcano is largely controlled by its fissure systems (Geist et al., 2005). Eruptive
 102 vents and fissures (Fig. 2b) show clear preferential orientations, with circumferential fissures
 103 around the summit caldera and radial fissures lower on its flanks (Chadwick and Howard, 1991).
 104 The radial fissure systems form diffuse rift zones, which are much wider than the rift zones
 105 observed at Hawaiian volcanoes (Geist et al., 2005). The WNW diffuse rift zone extends past the
 106 coast-line as a NW submarine ridge towards Roca Redonda (a mostly submarine volcano). The
 107 north diffuse rift zone also continues as a submarine ridge. The south diffuse rift zone is much wider
 108 (from SW to SE) but the youngest vents have a general SE orientation. The circumferential fissures
 109 consist of arcuate fissures, typically parallel to the caldera rim. Satellite observations of the
 110 vegetation distribution suggest that, in recent times, circumferential fissures have mostly been
 111 active on the eastern and southern quadrants (Fig. 2).

112 Table 1: Summary of Wolf historic activity (Modified from Schatz and Schatz, 1983 and Global
 113 Volcanism Program, 2013).

Eruption start	Eruption end	Intra-caldera vent	Circumferential fissure	Radial fissure	Explosive activity	Lava flow
Aug 1797						
21 Aug 1800		X			X	X
27 Sep 1849?	27 Sep 1849?					
26 Aug 1859	29 Aug 1859					
11 Apr 1925	26 Mar 1926			ESE		X
1933?				?		X?
Feb 1935						
1938?				?		X?
Jan 1948				SE (1200 m)	X	X
Mar 1963				SE (610 m)		X
28 Aug 1982	6 Sep 1982?	SW		SE (875 m)	X	X
25 May 2015	30 Jun 2015	S	SE (1580 m) to E (1635 m)		X	X

114

115 **2.3. Eruptive history**

116 The eruptive history of Wolf volcano is poorly constrained. Based on $^{40}\text{Ar}/^{39}\text{Ar}$ dating, Geist et al.
 117 (2005) proposed that the main episode of shield growth occurred over the last 100 ky but large
 118 analytical uncertainties prohibit detailed interrogation. Cosmogenic ^3He exposure dating suggests
 119 that the surface of Wolf is extremely young, perhaps only a few thousand years old, and comparable
 120 to the other Galápagos volcanoes with frequent historical activity (Reynolds et al., 1995; Naumann
 121 and Geist., 2000; Kurz and Geist, 1999). Geist et al. (2005) also suggest that Wolf suffered at least 2
 122 stages of caldera collapse, separated by a phase of caldera filling by lava flows. The surface of Wolf
 123 is mostly covered by ‘a‘ā lava deposits, with scarce pāhoehoe lava deposits. Historic activity in the
 124 last century is poorly constrained due to the remote location of the volcano but the most active area
 125 has been the SE flank, with at least 4 confirmed eruptions (Schatz and Schatz, 1983; Table 1). The
 126 1982 and 2015 eruptions are the only ones for which eyewitness accounts, field information and
 127 remote sensing data are available (Schatz and Schatz, 1983; Global Volcanism Program, 2013; Geist
 128 et al., 2005; Bernard et al., 2015).

129

130 **3. Methodology**

131 **3.1. Chronology**

132 The chronology of the 1982 eruption at Wolf is reconstructed using the available published
133 information and historic satellite imagery (Schatz and Schatz, 1983, Geist et al., 2005, Global
134 Volcanism Program, 2013), while the chronology of the 2015 eruption is based on new eyewitness
135 accounts, seismicity, field observations and satellite imagery time series (Supplementary Material
136 1).

137 In 2014 the Instituto Geofísico de la Escuela Politécnica Nacional (IG-EPN) installed a continuous
138 seismic monitoring network in the Western Galápagos that is composed of 6 broadband stations
139 located on Fernandina (2), Sierra Negra (2), Cerro Azul (1) and Alcedo (1). Data from this network
140 allow estimates of the magnitude and location of the largest events related to the 2015 eruption. To
141 gain a better understanding of the temporal distribution of eruption-related seismicity, we apply a
142 STA/LTA detector (short-term average/long-term average; Withers et al., 1998) to the vertical
143 component data at the nearest station (FER1), located 35 km SW of Wolf summit, between 01 April
144 and 31 July 2015. The majority of the detected events were either noise transients or related to
145 seismicity at nearby Fernandina or Sierra Negra volcanoes. However, we identify ~300 events that
146 can be related to Wolf, based on general characteristics of the waveforms, particle motions of first
147 arrivals pointing roughly NE, and S-wave – P-wave arrival lags of approximately 6 seconds. We
148 then submit these ~300 events to a hierarchical clustering scheme with a correlation threshold of
149 0.70 (Rowe et al., 2002). This results in 43 clusters from which we generate stacks to enhance
150 signal to noise. Finally, we cross-correlate the 43 stacks across the same period as before, and
151 identify a grand total of 465 events. This methodology provides a bird’s-eye view of major trends in
152 seismicity evolution (Fig. 4A).

153 We use NASA’s Ozone Monitoring Instrument (OMI) to construct a time series of SO₂ outgassing
154 throughout the eruption (e.g. McCormick et al., 2014). A mobile DOAS (Differential Optical
155 Absorption Spectrometry) transect was performed on 29 May during a helicopter overflight to
156 compare with the OMI time series (Fig. 4B). We then use thermal images and time series of
157 volcanic radiative power (VRP, in Watt) during the 2015 eruption (Fig. 4C), provided by the
158 MIROVA system (Coppola et al., 2016). In detail, following the approach of Coppola et al. (2013),
159 we use these data sources to estimate time averaged lava discharge rate (TADR) and erupted
160 volumes. Finally, comparison between six synthetic aperture radar (SAR) images acquired at
161 different stages of the eruptive activity by the European Commission’s Sentinel-1 satellite, allows
162 us to detect changes in SAR coherence and track the growth of the lava fields (e.g. Dietterich et al.,
163 2012). The emplacement of lava flows alters the scattering properties of the ground surface, causing
164 decorrelation of the coherence SAR images.

165 **3.2 Mapping**

166 The 1982 lava fields of Wolf (Fig. 5) are identified by comparing Landsat satellite images from
167 1978 and 1982, and mapped using the QGIS Openlayers plugin
168 (<https://github.com/sourcepole/qgis-openlayers-plugin>), which provides a high resolution (0.30
169 m/pixel) DigitalGlobe satellite image acquired on 26 December 2014. This map is coherent with an
170 eyewitness description of the terminal lava front and the upper fissure (Schatz and Schatz, 1983;
171 Geist et al., 2005). We map the 2015 lava fields (Fig. 6) using a combination of diverse datasets,
172 including: thermal and optical oblique photographs acquired during two helicopter overflights
173 (29/05/2015 and 12/06/2015), pre-eruption optical Landsat-8 (25/12/2014) and post-eruption
174 Sentinel-2 (21/02/2017, 20 m/pixel) satellite images, Sentinel-1 SAR coherence maps, and UAV
175 photogrammetry data acquired during post-eruption fieldwork (3-22/06/2017; 2 subsets imaging the
176 SE lava fronts and 3 covering the E lava fronts). This approach enables mapping of both the lava
177 fields and associated kipukas (areas surrounded but not covered by lava flows) in great detail. All
178 data analyses are carried out using an open-source geographic information system (QGIS;
179 <http://qgis.org>).

180 The thicknesses of the 1982 lava fields are estimated using the 30 m/pixel Advanced Land
181 Observation Satellite Phased Array type L-band Synthetic Aperture Radar (ALOS PALSAR) digital
182 elevation model (DEM), acquired between 2006 and 2011 and published by the Japanese Aerospace
183 Exploration Agency (JAXA). Lava flow thickness for the 2015 SE and E lava flows are obtained
184 using two techniques: (1) from field measurements using a TruPulse 360 laser rangefinder by
185 averaging 5 readings at 11 waypoints (supplementary material 2); (2) using topographic profiles
186 extracted from high resolution (~0.03 m/pixel) digital surface models (DSM) (Fig. 7, supplementary
187 material 2). Using the ALOS PALSAR DEM and QGIS zonal statistics plugin, it was possible to
188 calculate the volume required to inundate the caldera floor, thus reproducing the 2015 intra-caldera
189 lava field area.

190

191 **3.3 Scoria and cryptotephra characterization**

192 Calculating the density and porosity of scoria associated with explosive activity and lava
193 fountaining during the 2015 eruption was not possible using classical techniques, such as paraffin
194 coating and measurements using Archimedes' principle, due to the extreme fragility of the samples.
195 We instead calculate the volume of an ellipsoidal envelope of the size of the 3 major axes of the
196 clasts and estimate the scoria volume using the ellipsoidal envelope volume and a correction factor
197 for the linear relationship between ellipsoid and measured volume of 1700 pyroclasts
198 (Supplementary material 3). The scattering of the linear relationship, expressed as two standard
199 deviations, is then used as an error estimate. The scoria mass is measured on a 10^{-2} g resolution

200 electronic scale to determine its density. The scoria porosity is calculated using a grain density
201 obtained by water pycnometry on scoria powder, milled with an automatic agate mortar.

202 Cryptotephra was collected on 11 June in Quito in a homemade ashmeter (Bernard, 2013) that was
203 installed on the roof of the IGEPN in anticipation of the Cotopaxi unrest. The ashmeter allows the
204 collection of sub-millimeter deposits of ash with low ambient contamination or reworking. The
205 cryptotephra was compared to the scoria found on Wolf volcano using an Olympus SZ61 binocular
206 microscope.

207

208 **4. Chronology of the Wolf eruptions**

209 ***4.1. The 1982 eruption***

210 There is no information regarding possible unrest before the 1982 eruption at Wolf volcano, due to
211 the absence of a monitoring system in the Galápagos Archipelago at this time. The eruption started
212 on 28 August 1982 with a low altitude gas plume (~4 km), which was first detected by satellite
213 images between 13h00 and 14h00 LT (local time = Universal Time Coordinated UTC – 6; Global
214 Volcanism Program, 2013). The first eyewitness account was made at 16h45 LT by the captain of
215 the *La Encantada* cruise ship (Schatz and Schatz, 1983). The eruption was characterized by two
216 main vents: one inside the caldera, which was observed first, and one on the SE flank, observed on
217 the second day. According to estimates from the Nimbus-7 TOMS satellite, the eruption produced
218 $1.08\text{E}+9$ kg of SO₂ on 29 August (Global Volcanism Program, 2013). Schatz and Schatz (1983)
219 describe the lava flow from the SE flank as a typical ‘a‘ā flow, ~200 m-wide, flowing at only 0.5-1
220 m/h at the time of their visit on 30 August. They estimate the thickness to be 3–4 m at the flow
221 margin and up to 7 m in the middle of the flow. Activity on the SE flank stopped on 1 September.
222 According to Schatz and Schatz (1983), activity from the intra-caldera vent began on 28 August and
223 strengthened after the end of the activity from the SE fissure. Intra-caldera activity occurred from a
224 fissure on the SW side of the caldera floor, created a new cone, and covered ~6 km² of the caldera
225 floor with >5 m thick ‘a‘ā flows (Geist et al., 2005). During the night of 3 September, the lava
226 fountain from the caldera vent reached 700-800 m high (i.e. higher than the caldera rim), leaving
227 scoria deposits on the western bench. The eruption lasted at least until 6 September, and possibly
228 until 16 October 1982 (Schatz and Schatz, 1983).

229

230 ***4.2. The 2015 eruption***

231 ***4.2.1. Precursory activity***

232 As of the time of writing, as well as at the time of the 2015 eruption, no dedicated ground-based
233 monitoring system is in place at Wolf volcano. However, interferometric synthetic aperture radar

234 (InSAR) observations provide critical constraints on the extent and location of ground deformation
 235 prior to the 2015 eruption (Stock et al., in review). The edifice showed a total of 0.6 m inflation
 236 between 1992 to 2009, associated with a source location below the summit caldera (Bagnardi,
 237 2014). The inflation stopped between 2009 and the end of 2010. Then routine SAR data collection
 238 stopped until shortly before the 2015 eruption (Stock et al., in review).

239 The majority of seismicity related to the 2015 unrest and eruption at Wolf was too small to be
 240 located by the IG-EPN Galápagos seismic array. Using the FER1 station, a total of 465 earthquakes
 241 were detected and allow a better characterization of the eruptive process. The first earthquake
 242 considered to mark the start of seismic unrest immediately preceding the eruption was detected at
 243 08h28 LT on 24 May 2015. Subsequent earthquakes were separated on an approximately hourly
 244 timescale until 18h52 LT on 24 May, when the frequency increased to one earthquake every ~30
 245 minutes. Then, at 23h30 LT on 24 May, the frequency increased further to one earthquake every <5
 246 minutes. Before 23h50 LT on 24 May, the earthquakes were very small (magnitude probably ≤ 2)
 247 making them impossible to identify on stations other than FER1. After this time, earthquakes were
 248 detected by other stations in the array and a total of 9 events ranging in magnitude between 2.1 –
 249 4.4 were successfully located on the NE flank of Wolf (Table 2), albeit with significantly large
 250 horizontal errors (~21 km). The earthquake at 00h58 LT was the most energetic and is thought to be
 251 associated with an explosion at the onset of the eruption (Bernard et al., 2015).

252

253 Table 2. Located seismic events during the unrest and start of the 2015 eruption of Wolf volcano.
 254 LT: Local Time = UTC – 6 hours.

Date	Hour (LT)	Latitude	Longitude	Magnitude
24 May 2015	23:50:16	0.080310	-91.309450	3.3
25 May 2015	00:06:40	0.064950	-91.306290	2.4
25 May 2015	00:09:51	0.069820	-91.306820	2.1
25 May 2015	00:16:43	0.095710	-91.310440	3.5
25 May 2015	00:20:19	0.103320	-91.294740	2.8
25 May 2015	00:21:20	0.071190	-91.321980	2.5
25 May 2015	00:33:25	0.058620	-91.308400	3.0
25 May 2015	00:58:35	0.077760	-91.327510	4.4
25 May 2015	01:16:50	0.093270	-91.302550	2.2

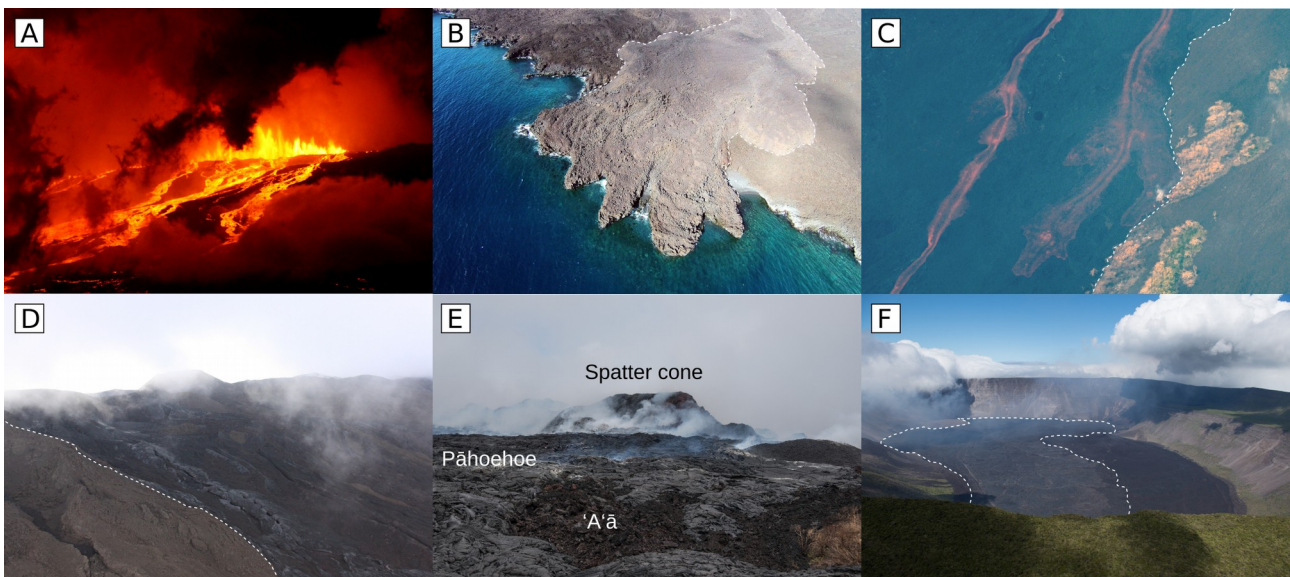
255

256

257 4.2.2. Eyewitness accounts and eruption development

258 Dr. David Anchundia (Charles Darwin Foundation) was monitoring Mangrove finches at Tortuga
259 Negra beach on the west side of Isabela Island at the start of the eruption and reports that activity
260 began between 00:30 and 00:45 LT on 25 May 2015. The group woke up after an earthquake
261 (possibly the one recorded at 00h33 LT) and saw the volcano erupting. They recorded video footage
262 of the eruption at 00:50 LT. In this footage the eruption is already well developed with intense lava
263 fountaining and lava flows descending the SE flank. A very intense hot spot was first observed on
264 Wolf volcano by the Hawai'i Institute of Geophysics and Planetology (HIGP) at 01:28 LT, based on
265 GOES 8/10 satellite information. The eruption was also observed by a cruise ship (*La Pinta*), which
266 was sailing off the eastern coast of the volcano and first reported the eruption at 01:29 LT (Fig. 3A).
267 Analysis of the video footage and pictures from the eruption suggests that the initial lava fountain
268 was 100-150 m high and was fed by a >800 m long circumferential fissure located on the upper SE
269 flank. At 02:15 LT, the Washington Volcanic Ash Advisory Center (VAAC) reported a 10.7 km high
270 plume moving SW. Two further plumes were reported at 03:45 LT: one at 15.2 km above sea level
271 (a.s.l.) moving E-NE, the other at 13.7 km a.s.l. moving south. Eye-witnesses report numerous
272 episodes of lightning within the eruptive plume.

273
274

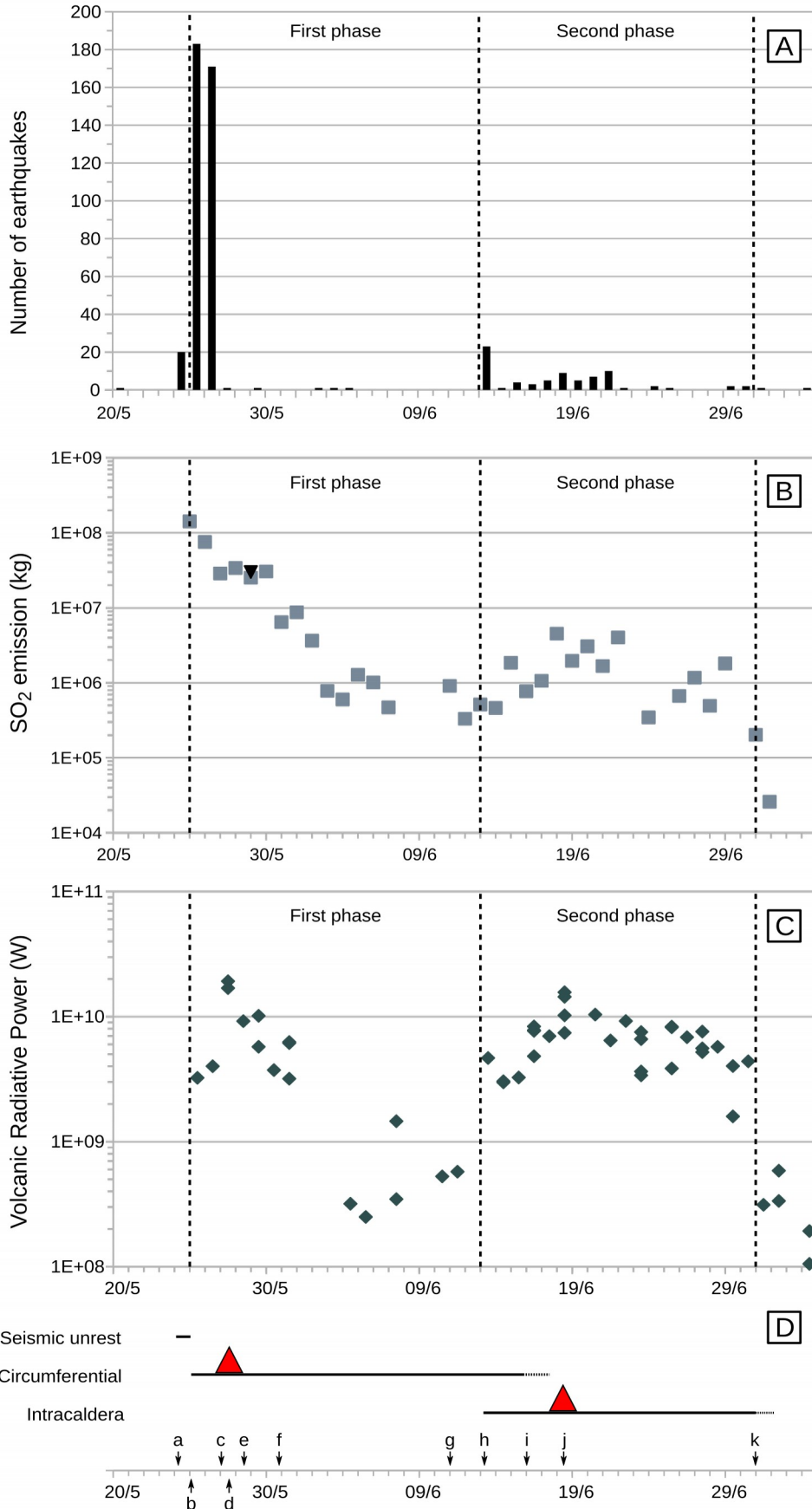


275 Figure 3. Photographic accounts of the 2015 eruption of Wolf volcano. A: a lava fountain from the
276 circumferential fissure on 25 June (courtesy of the *La Pinta* crew); B: a lava delta that reached the
277 sea between 26 and 27 June; C: active lava flows on the eastern flank on 29 June; D: a
278 circumferential fissure still active on June 12; E: pāhoehoe and 'a'ā lava deposits close to the
279 circumferential vent (courtesy of the Galápagos National Park: PNG); F: no activity was observed
280 on 1 July and the new intra-caldera lava field (outlined by a white dashed line) is not active
281 anymore (courtesy of the PNG).

282 During the first phase of the eruption (25 May – 12 June), the active vents shifted rapidly from the
283 SE side of the outer rim of the caldera to the E side and were located along a circumferential fissure
284 with a total length of 2.8 km. On the first day, the eruption emitted about $1.23\text{--}1.42\text{E}+8$ kg of SO_2
285 (Fig. 4, Supplementary Material 1). Seismic activity was intense and almost continuous until 27
286 May, after which it decreased rapidly. According to the thermal anomalies, the peak activity for this
287 phase occurred on 27 May (Fig. 4, Supplementary Material 1). The lava flows emitted from the E
288 fissure probably reached the sea between 26 and 27 May (Fig. 3B). On 28 May, the gas plume
289 extended over 3000 km and passed above mainland Ecuador. During a helicopter overflight on 29
290 May, IG-EPN members measured >500 °C Maximum Apparent Temperatures (MAT) at vents
291 located at the N end of the circumferential fissure using an infrared camera, and observed active
292 lava flows on the E flank of the volcano (Fig. 3C). The same measurements made at vents at the S
293 end of the circumferential fissure gave temperatures of 45 °C (MAT), indicating that it was no
294 longer active. Both SO_2 emissions and thermal anomalies slightly increased between 30 and 31
295 May, before decreasing rapidly. From 3 to 10 June, the eruption intensity dropped significantly. On
296 5 June, a Landsat-8 satellite image showed that the activity was still focused on the northern part of
297 the circumferential fissure but limited to 5 active vents that were not producing significant lava
298 flows. The eruption resumed on 11 June when large thermal anomalies were detected from the
299 circumferential fissure, associated with renewed SO_2 emissions but without any significant seismic
300 activity. The active area was about 2.2 km-long and, according to Landsat-8 imagery, mostly fed the
301 E lava field. On 12 June, during a PNG-led field visit to assess the health of the pink iguana
302 population on the northern side of the caldera, members of the IG-EPN noted that the E and SE lava
303 fields were still active (Fig. 3D) and heard several explosions from circumferential vents. MAT of
304 86.1 °C and 96.8 °C were measured in lava flows on the SE and E flanks of the volcano,
305 respectively. At the N end of the circumferential fissure, MAT >500 °C were measured at vents
306 which continued to emit lava towards the E flank. IG-EPN members also observed that the caldera
307 area was not active at that time. Pictures from a helicopter overflight by the PNG park rangers on 1
308 July revealed that the circumferential area was covered by both ‘a‘ā and pāhoehoe lava flows and
309 had several new spatter and scoria cones (Fig. 3E). According to InSAR data analyses and
310 petrological geobarometry, this first (circumferential fissure) phase of the eruption was
311 accompanied by edifice-wide deflation due to magma extraction from a lower crustal storage
312 region, with intra-caldera deformation suggesting associated deflation of a small shallow sill (Xu et
313 al., 2016; Stock et al. in review).

314 The second phase of the 2015 eruption started on 13 June when the activity shifted to a vent within
315 the caldera, located 2.6 km west of the circumferential fissure and 1 km east from the 1982 intra-
316 caldera vent (Fig. 6). This intra-caldera activity is evident in the seismic record as a swarm of
317 earthquakes from Wolf volcano started at 03h01 LT on 13 June, unfortunately none of them was

318 large enough to be located. After the opening of the intra-caldera vent, activity from the
319 circumferential fissure progressively waned and was mostly over by 16 June. Thermal anomalies
320 and SO₂ emissions indicate that the peak in activity from the caldera vent occurred on 18 June,
321 without an obvious increase in seismic activity. Thermal energy released on June 18 was almost as
322 high as the peak in the circumferential fissure activity on the 27 May, but the SO₂ flux was 6 times
323 lower. The SO₂ emissions, seismicity and thermal anomalies strongly decreased until the end of
324 June. SAR coherence maps show that the caldera lava field was still growing between 23 June and 5
325 July. Edifice-wide deflation measured by InSAR during the second phase of the eruption is
326 consistent with magma extraction from the same lower crustal storage region that fed the first phase
327 (Xu et al., 2016; Stock et al., in review). Minor thermal anomalies were detected after 30 June and
328 are probably associated with the cooling lava fields. No SO₂ emissions were detected by satellites
329 after 1 July. According to observations by the PNG rangers, the caldera lava field was inactive on 1
330 July (Fig. 3F). Hence, the eruption had mostly stopped by 30 June and had a total duration of 36
331 days.



333 Figure 4. Evolution of the 2015 eruption of Wolf volcano. A: daily number of earthquakes detected
 334 by the FER1 broadband station. B: SO₂ emissions through time. Grey squares show emissions
 335 detected by OMI, black triangle corresponds to a mobile-DOAS flux (3.1E+7 kg/day) measurement

336 obtained during the helicopter overflight on 29 May. C: Volcanic Radiative Power obtained by
337 MIROVA. D: Timeline of the eruption with main events as follows; a: seismic unrest detected at
338 08h28 LT on 24 May; b: eruption starts from the southern part of the circumferential fissure at
339 ~00h33 LT on 25 May; c: lava from the E field reaches the sea between 26 and 27 May; d: first
340 phase, highest peak of activity on 27 May according to the thermal anomalies (red triangle on the
341 circumferential timeline); e: gas plume reaches mainland Ecuador on 28 May; f: first phase, second
342 peak of activity between 30 and 31 May; g: renewed activity from the northern part of the
343 circumferential fissure on 11 June; h: eruption starts from the caldera vent with seismic activity
344 starting at 03:01 LT on 13 June; i: waning of the activity from the circumferential fissure on 16
345 June; j: second phase, highest peak of activity on 18 June (red triangle on the intracaldera timeline);
346 k: waning of the activity from the caldera vent on 30 June.

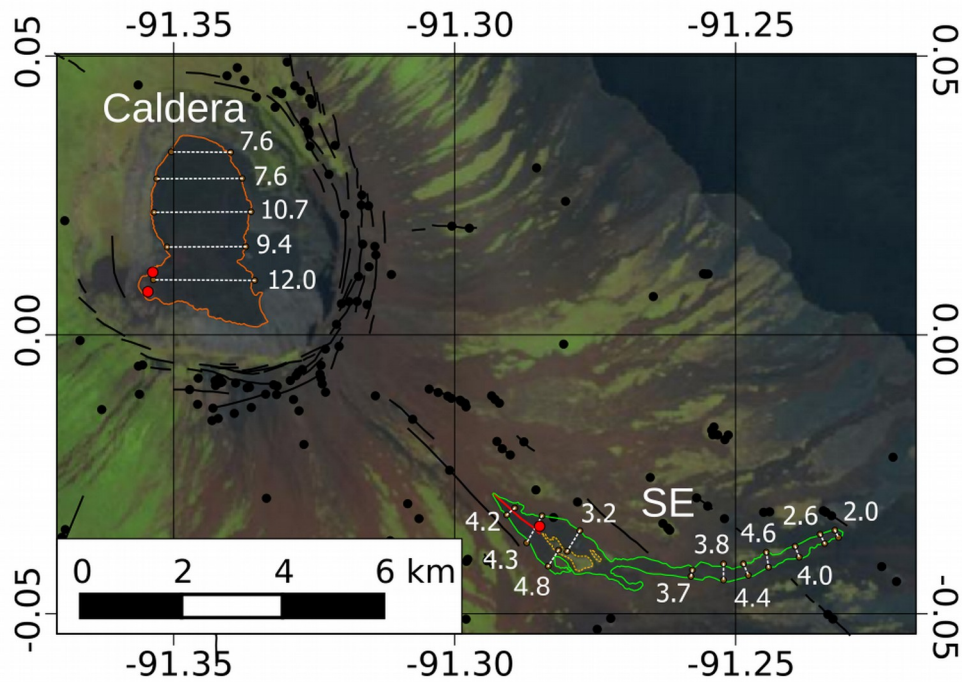
347

348 **5. Eruption products**

349 **5.1. 1982 Lava fields**

350 The 1982 SE vent occurred as a 1.2 km-long radial fissure located at an elevation of 875 m and
351 produced an ‘a‘ā lava field that reached ~250 m a.s.l. This flow is 7.2 km long, up to 1 km wide and
352 covers an area of ~2.71 km², including 0.19 km² of kipuka (Fig. 5). The mean thickness estimated
353 from 11 topographic profiles from the ALOS-PALSAR DEM (Fig. 5; Supplementary Material 2)
354 along the 1982 SE lava field is 4.0 ± 1.6 m between the front of the flow and the vent area, in
355 agreement with Schatz and Schatz (1983). From the high resolution satellite images, it appears that
356 the 1982 intra-caldera lava field (6.16 km²) is mainly an ‘a‘ā lava deposit with a little area of
357 pāhoehoe lava deposit that was emplaced later during the eruption at the eastern margin. The
358 pāhoehoe appears to be fed by lava tunnels inside the ‘a‘ā lava field and could be related to the
359 waning phase of the eruption (between 6 September and 16 October) as it was not described by
360 eyewitnesses on 3 September. From topographic measurements, the 1982 intra-caldera lava deposit
361 thickness ranges 7.6-12 m, in agreement with the field estimates of Geist et al. (2005). Hence, the
362 total volume of lava deposits produced during the 1982 eruption is $70.0 \pm 23.0E+6$ m³, with $10.0 \pm$
363 $4.1E+6$ m³ from the radial fissure and $60.0 \pm 18.9E+6$ m³ from the caldera vent (Table 2,
364 Supplementary Material 2). This result carries a large uncertainty because there is no accurate
365 information on the pre-1982 caldera floor topography and because of the low resolution (30
366 m/pixel) of the ALOS-PALSAR DEM.

367



369 Figure 5. Distribution of lava fields and vents from the 1982 eruption of Wolf volcano. Background:
 370 Landsat image acquired on 16/05/1991; Caldera: caldera lava field; SE: southeast lava field; red
 371 dots: cones built during the eruption; red line: radial fissure; yellow dotted outlines: kipukas.
 372 Thickness values in white correspond to average thicknesses measured on the JAXA ALOS-
 373 PALSAR DEM (Supplementary Material 2).

374

375 The uncertain end date of the 1982 eruption (either 6 September or around 16 October) precludes
 376 any accurate determination of the eruption rate. However, eyewitness accounts suggest that most of
 377 the lava emissions occurred between 28 August and 6 September, giving an average eruption rate of
 378 47.1-97.7 m³/s (bulk deposit).

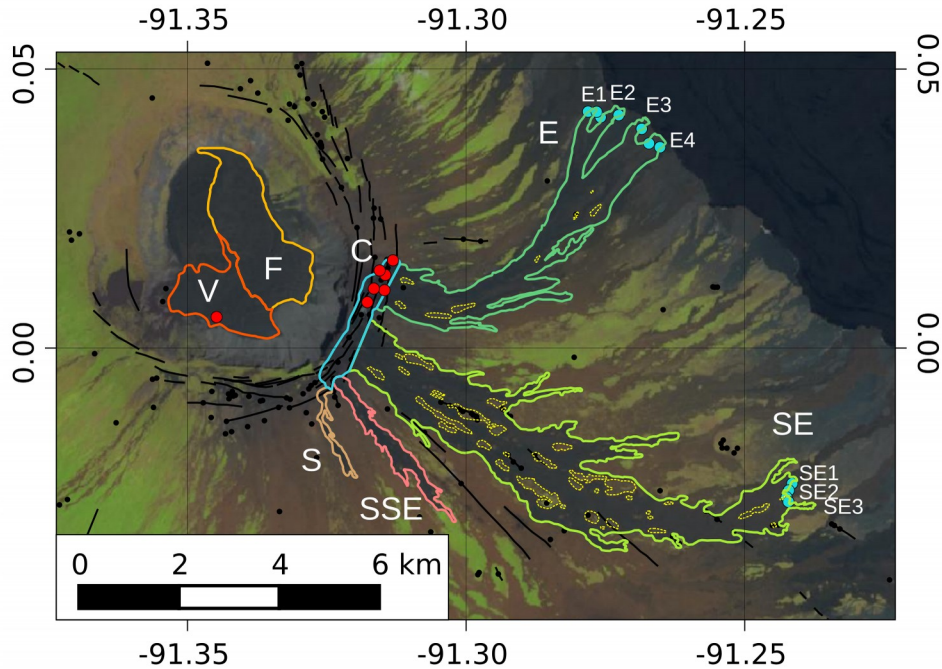
379

380 **5.2. 2015 Lava fields**

381 Lava fields associated with the 2015 eruption on Wolf cover a total subaerial area of 25.42 ± 1.17
 382 km², which includes 1.43 ± 0.36 km² of kipukas (Fig. 6). The E lava field reached the sea but did
 383 not create a large lava delta, so we assume that the volume of the submarine lava deposit is
 384 negligible compared to the subaerial deposits. In order to estimate the average thickness of the
 385 deposits, we divided them into 7 geographically separate lava fields (Fig. 6): 1) circumferential
 386 fissure deposits (C; 2.9 km long, 400 m wide); 2) south lava field (S; 1.8 km long, up to 180 m
 387 wide); 3) south-southeast lava field (SSE: 3.7 km long, up to 500 m wide); 4) southeast lava field
 388 (SE: 10 km long, up to 2 km wide); 5) east lava field (E: 6.8 km long, up to 1.1 km wide); 6)
 389 caldera vent deposits (2.2 km long, up to 1.1 km wide; and 7) caldera floor lava field (3.5 km long,

390 up to 1.5 km wide). The circumferential fissure (C) is the origin of the flank lava fields (S, SSE, SE
 391 and E). The activity from the caldera vent covered part of the 1982 intra-caldera lava field but also
 392 filled a depression to the east. Most of the lava flows were ‘a‘ā deposits except part of the
 393 circumferential area and possibly part of the caldera floor area, which are pāhoehoe.

394
 395



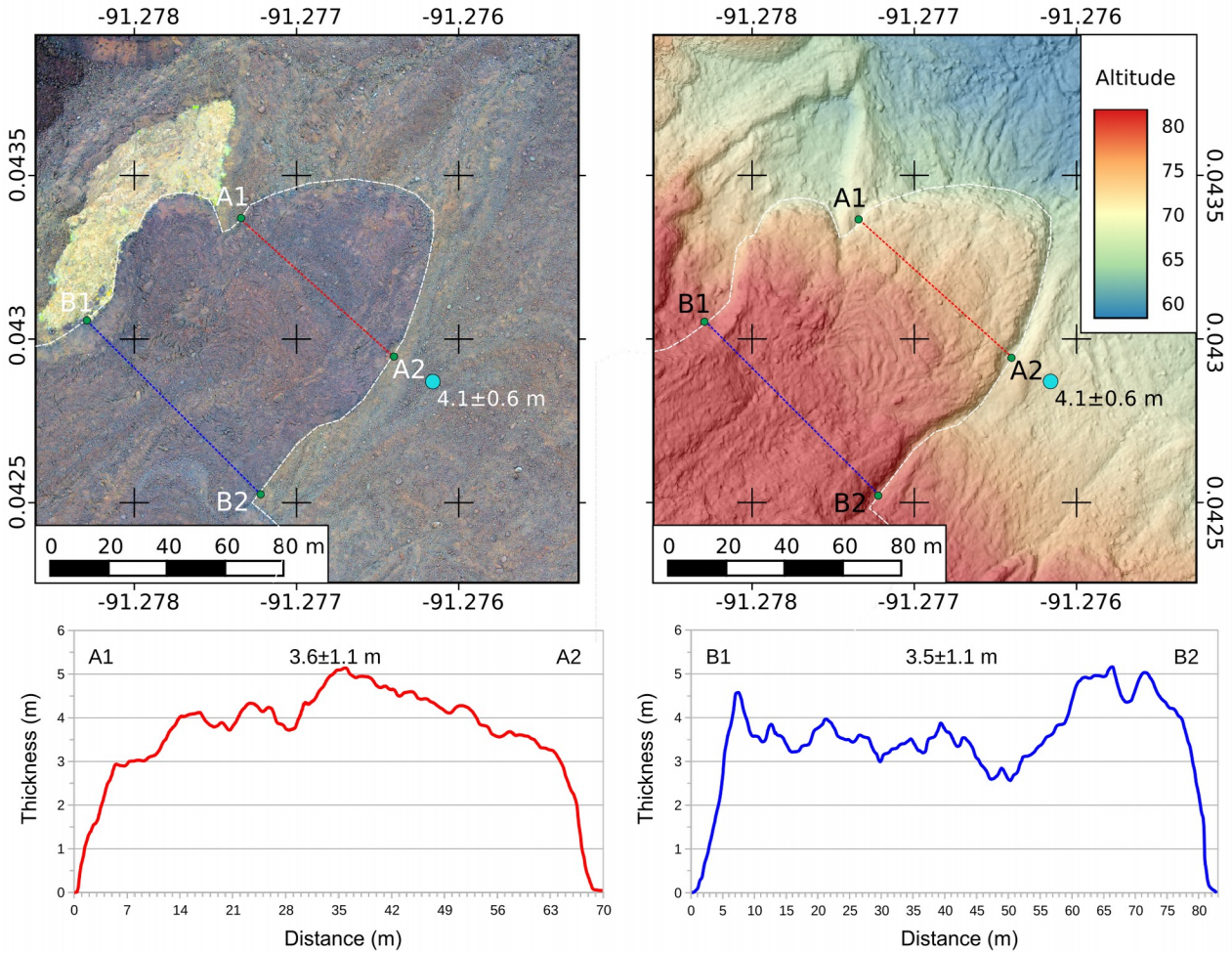
396 Figure 6. Distribution of lava fields and vents from the 2015 eruption of Wolf volcano. Background:
 397 Sentinel-2 image acquired on 21/02/2017; C: Circumferential fissure area; S: south lava field; SSE:
 398 south-southeast lava field; SE: southeast lava field; E: east lava field; V: caldera vent area; F:
 399 caldera floor lava field; blue dots: field thickness measurements; red dots: vents active on satellite
 400 images; yellow dotted outlines: kipukas; L: lava lobes at flow front (thickness values in
 401 Supplementary Material 2).

402

403 In general, we found out that the field measurements, made on the margins of the deposits, slightly
 404 overestimate (~0.5 m) the average thickness of the lava deposits compared with the high-resolution
 405 DSM (Fig. 7, Supplementary Material 2). Profiles from the same lobe show relatively constant
 406 average thicknesses and can be used as a good approximation of the deposit thickness. The standard
 407 deviation of the thickness in each profile provides a reasonable error estimate, resulting from
 408 uncertainty in the pre-eruptive topography. Although we don't have direct field measurements along
 409 the entire flows (i.e. upstream), we assume that the thickness would be relatively constant along the
 410 flows as observed for the 1982 SE lava field (Fig. 6). Furthermore, the slope of lower flank at lobes
 411 E1 (12°) and E2 (11°) in the E lava field, and lobe SE3 (5°) in the SE field (Fig. 6), are close to the
 412 global slope (from fissure to lava front) of their respective lava field (13.5° for the E field and 7° for

413 the SE field). Only the lobe E3 (5°) has a slope significantly below that of the overall lava field. The
414 average thicknesses from the SE lobes are very similar (2.4-2.7 m) while the thicknesses from the E
415 lobes are much more variable (3.5-6.7 m). We suggest that this is related to the timing of
416 emplacement of the different lobes. According to the SAR coherence maps, the SE lava field was
417 emplaced before 30 May, while part of the E lava field (in particular the E1 and E2 lava lobe) was
418 emplaced between 30 May and 11 June. To estimate the average thickness for each lava field, we
419 used the average profile thicknesses weighted by the length of each profile. This gives an average
420 thickness of 2.5 ± 0.8 m and 5.2 ± 1.5 m for the SE and E lava fields, respectively (Supplementary
421 Material 2). These results are similar to other Galápagos flank eruptions, such as Fernandina 1995
422 (8.5 ± 2 m) and Cerro Azul 2008 (4.5 ± 2 m; Rowland et al., 2003). We assume the same average
423 thickness for the S, SSE and SE lava field as they were emplaced during the same eruptive phase
424 and therefore probably had a similar viscosity and discharge rate. However, due to the lack of direct
425 measurements on the S and SSE field, we assume a conservative 50% error, slightly higher than the
426 standard deviation on the SE lobes average thickness. In the absence of direct or DSM
427 measurements, we estimate the thickness of the circumferential fissure area to be intermediate
428 between the E and SE lava field with a 50% error (4.0 ± 2 m). Photographs from this area (Fig. 3E)
429 support this approximation which is similar to the 1982 radial fissure area (4.3 ± 1.7 m).

430 The minimum average thickness necessary to reproduce the lava field in the caldera floor area is
431 calculated as 7 m, with a maximum thickness in the ponding area of 17 m. These results predict a
432 maximum 5 m thick deposit at the margins. Considering the margin thicknesses measured for the
433 1982 intra-caldera lava field (up to 10 m), which are similar to the margin thickness measured for
434 the intra-caldera lava field of the 2005 eruption of Sierra Negra (Geist et al., 2008), we propose the
435 average thickness of the caldera floor lavas to be 9.5 ± 2.5 m. In the absence of topographic
436 constraints on the intra-caldera vent area where no ponding happened, we used the same thickness
437 value for the caldera vent area with a conservative 50% error (average thickness of 9.5 ± 4.8 m).



439 Figure 7. High resolution orthomosaic and digital surface model and corresponding topographic
 440 sections of the SE lava field lobe E1 (location in Fig. 6).

441

442 The total volume of lava deposits produced during the 2015 eruption of Wolf volcano is $116.0 \pm$
 443 $45.0E+6 \text{ m}^3$, with $63.4 \pm 25.1E+6 \text{ m}^3$ from the first (circumferential fissure) phase and $52.6 \pm$
 444 $19.9E+6 \text{ m}^3$ from the second (caldera vent) phase. Hence, the 2015 eruption was approximately
 445 65% larger than the 1982 eruption (Table 2). The average eruption rate for the 2015 eruption is
 446 $22.5\text{-}50.8 \text{ m}^3/\text{s}$ (bulk deposit); this is smaller than the 1982 eruption but includes 8 days of low
 447 activity (3 to 10 June).

448 Based on the detailed morphology of the 2015 ‘a‘ā lava lobes it is possible to obtain some
 449 rheological constrains near flow cessation (Supplementary Material 2). Using empirical formulae
 450 (Jeffrey, 1925; Nichols, 1939), we estimated a viscosity for the SE and E lava lobes to be 3.56-
 451 $4.56E+5 \text{ Pa}\cdot\text{s}$ and $4.17\text{-}19.7E+6 \text{ Pa}\cdot\text{s}$, respectively. These values are typical of ‘a‘ā lava flows
 452 (Belousov and Belousova, 2018 and references therein). As no bulk composition difference was
 453 observed between the SE and E lava fields (M.J. Stock unpublished data), the large difference in
 454 viscosity is probably due to a combination of factors that include the slope, the discharge rate and
 455 the cooling history. Lower viscosity for the E flows is probably associated to colder lava and higher

456 crystal content. Using the equation of Hulme (1974), the yield strength of the SE and E lava lobes is
 457 estimated in $5.23-5.56E+3$ and $1.52-2.60E+4$ Pa, respectively. Using the equation of Jeffrey (1925),
 458 we estimated a velocity for the SE lobe of 1.51-1.71 m/s, which compares very well with the
 459 velocity of the lava flows calculated from the thermal satellite image from 2h00 LT on 25 May,
 460 when the flow traveled 7.5 ± 1 km in about 1h30 (average velocity 1.2-1.6 m/s). The E lava lobes
 461 morphology suggests much lower velocities (0.11-0.24 m/s), consistent with the time taken for the
 462 lava flow to reach the ocean (~ 24 hours, average velocity 0.08 m/s).

463

464 Table 2 Summary of parameters for the 1982 and 2015 eruptions of Wolf volcano. Eruption rate
 465 values in bulk deposit (DRE = bulk*0.75 assuming 25% void).

	1982	2015
Flank lava field	Radial fissure (SE, ~ 875 m a.s.l.)	Circumferential fissure (SE-E; $\sim 1580 - \sim 1635$ m a.s.l.)
Area (without kipukas)	2.52 ± 0.14 km ²	18.46 ± 1.35 km ²
Thickness	4.0 ± 1.6 m	3.4 ± 1.4 m
Volume	$10.0 \pm 4.1E+6$ m ³	$63.4 \pm 25.1E+6$ m ³
Duration	3-4 days	~ 20 days
Average eruption rate	17.0-54.3 m ³ /s	22.1-51.2 m ³ /s
Caldera lava field	SW vent (~ 1027 m a.s.l.)	S vent (~ 1012 m a.s.l.)
Area	6.16 km ² ± 0.31 km ²	5.54 km ² ± 0.17 km ²
Thickness	9.7 ± 3.0 m	9.5 ± 3.6 m
Volume	$60.0 \pm 18.9E+6$ m ³	$52.6 \pm 19.9E+6$ m ³
Duration	9 days (minimum)	~ 18 days
Average eruption rate	52.8-101.4 m ³ /s (maximum)	18.9-42.0 m ³ /s
Total		
Area	8.68 ± 0.45 km ²	24.00 ± 1.52 km ²
Thickness	8.1 ± 2.9 m	4.8 ± 2.0 m
Volume	$70.0 \pm 23.0E+6$ m ³	$116.0 \pm 45.0E+6$ m ³
Duration	9 days (minimum)	36 days
Average eruption rate	60.4-119.5 m ³ /s (maximum)	22.8-51.8 m ³ /s

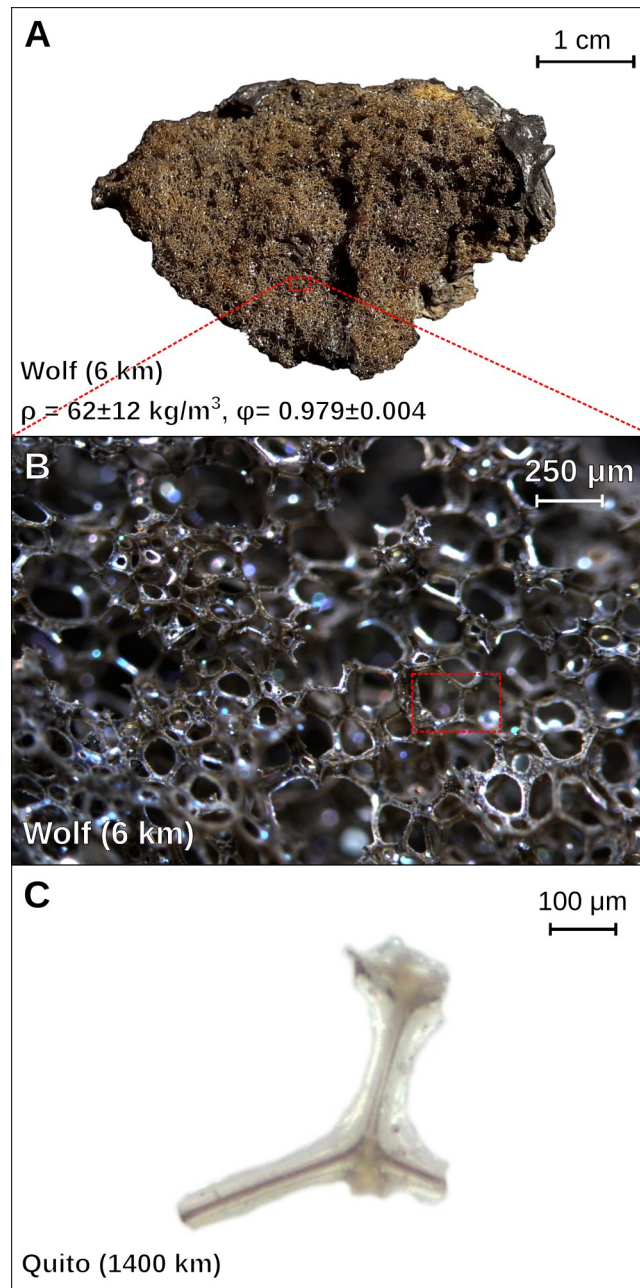
466

467

468 *5.3. Reticulite and cryptotephra in Quito*

469 On 11 June 2015, one 0.5 mm-diameter glassy fragment with a polygonal lattice was collected in an
470 ashmeter installed on the roof of the IG-EPN, in Quito. This sample was compared with the fresh
471 scoria found on the eastern flank of Wolf volcano during the 2017 field campaign (Fig. 8). The
472 scoria samples have a similar glassy texture with a characteristic lattice structure typical of
473 reticulite. The scoria bulk density ranges from 56 ± 23 to 76 ± 32 kg/m³ and their porosity ranges
474 from 97.3 ± 1.1 to 98.0 ± 0.8 %, using a grain density of 2782 kg/m³ measured by water
475 pycnometry. The grain density is consistent with the melt density (~ 2713 kg/m³) at atmospheric
476 pressure, calculated using the average glass composition (assuming near-complete degassing on
477 ascent [<0.1 wt% H₂O] and a pre-eruptive temperature of 1150 °C; Lange and Carmichael, 1990;
478 Stock et al., in review). Scoria was not found on top of the 2015 lava fronts, suggesting that the
479 scoria fallout occurred before 27 May, when the east lavas arrived at the shoreline, which is
480 consistent with the arrival of the gas plume over Ecuador (28 May). We measured the scoria size in
481 4 different locations and found the largest clast (10.9 cm) at 6.4 km NE of the vent, while the scoria
482 were only 2.4-3.6 cm-diameter between 9.4 and 11 km E and SE of the vent. No ash deposits were
483 found associated with the scoria in the field. IG-EPN operators did not observe any tephra deposits
484 during a visit to the northern rim of the caldera on 12 June 2015. The almost complete absence of
485 crystals in the reticulite samples allows us to use its glass composition and pre-eruptive conditions
486 (1150 °C, Stock et al., in review) to calculate the melt viscosity (Giordano et al., 2008). The melt
487 viscosity is $\sim 2.3E+2$ Pa.s (assuming <0.1 wt% H₂O due to efficient degassing during ascent), which
488 is 3 to 5 order of magnitude lower than the viscosity estimated near flow cessation. Low viscosity is
489 assumed in the formation of reticulite ($1E+2$ Pa.s in Mangan and Cashman, 1996). This result is
490 consistent with the viscosity of Cerro Azul melts ($2E+2$ Pa.s) calculated by Naumann and Geist
491 (2000), and could significantly reduce the uncertainty on the Cerro Azul and Fernandina effusion
492 rates calculated by Rowland et al. (2003). Large differences between viscosity calculated by
493 petrology and flow morphology have also been observed for Icelandic basaltic flows (Chevrel et al.,
494 2013) and testifies the major change of viscosity that occurs when the lava reach the surface
495 because of rapid cooling and crystallisation. Also, in this case, as well as small crystals forming in
496 the lava as they cool, the lavas have a higher phenocryst load than the reticulite.

497



499 Figure 8. Glassy samples from the 2015 Wolf eruption. A) and B) Reticulite scoria found on the
 500 eastern flank of Wolf volcano. C) Cryptotephra fragment collected in Quito on 11 June 2015, 1400
 501 km from Wolf volcano.

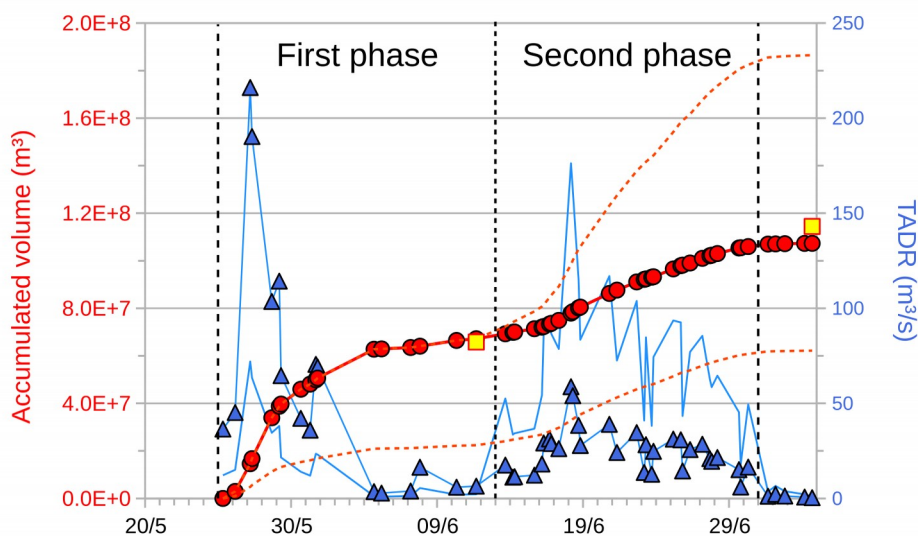
502

503 **5.4. Time Average Discharge Rate**

504 Using the MIROVA time series of Volcanic Radiative Power (Fig. 4) and an average melt SiO_2
 505 content of 48.8 wt. % (Stock et al., in review), we calculated the radiant density (c_{rad}) of $\sim 1.8\text{E}+8$
 506 J/m^3 , or between ~ 0.9 and $\sim 2.7\text{E}+8 \text{ J/m}^3$ considering the $\pm 50\%$ accuracy of the empirical fit
 507 (Coppola et al., 2013). Accordingly, we calculate a bulk volume of $62\text{-}186\text{E}+6 \text{ m}^3$, which is in
 508 excellent agreement with post-eruption field-based estimate of $71\text{-}161\text{E}+6 \text{ m}^3$. The comparison with
 509 field-derived volumes (Fig. 9) suggests that the two eruptive phases (circumferential and intra-

510 caldera) were characterized by two distinct radiant densities that are likely associated with
 511 differences in topography and emplacement conditions. In detail, we found that the lava flows
 512 emplaced on the E and SE flanks of the volcano during the first phase were characterized by a
 513 radiant density at the lower boundary ($\sim 0.9\text{E}+8 \text{ J/m}^3$), while the lava field emplaced inside the
 514 caldera during the second phase was characterized by the radiant density at the higher boundary
 515 ($\sim 2.7\text{E}+8 \text{ J/m}^3$). Accordingly, the initial phase had the highest time average discharge rate (TADR)
 516 with an initial peak of $216 \text{ m}^3/\text{s}$ (bulk deposit) on 27 May 2015 that probably corresponds to the
 517 high lava fountaining phase, which produced the reticulite tephra. Phase 2 was characterized by
 518 lower TADR that reached a maximum value of $59 \text{ m}^3/\text{s}$ (bulk deposit) on 18 June 2015, in
 519 agreement with the much lower SO_2 emission (Fig. 4).

520
521



522 Figura 9. Accumulated volume and calculated time averaged discharge rate (TADR). Dotted orange
 523 line: range of VRP-derived accumulated volume using the range of radiant densities; yellow
 524 squares: field-based accumulated volume; red circles: VRP-derived accumulated volume that best
 525 fits the field observations and SO_2 emissions; blue lines: range of time average discharge rate
 526 (TADR) using the range of radiant densities; blue triangles: TADR using the best fit to field
 527 observations and SO_2 emissions.

528

529 6. Discussion

530 6.1. Unrest at western Galápagos shield volcanoes

531 Our detailed analysis of the 1982 and 2015 Wolf eruptions provides new constrains on the eruptive
 532 dynamics of large western Galápagos shield volcanoes. The 2015 Wolf unrest is similar to recent
 533 periods of unrest at Fernandina (September 2017 and June 2018), in which a series of M2.5-4.1
 534 earthquakes occurred over a few hours before the eruptions with only small-scale ground

535 deformation (Vásconez et al., 2018). On the other hand, these are distinct from the recent seismic
536 activity and large-scale ground deformation recorded at Sierra Negra before the June-August 2018
537 eruption. In the case of Sierra Negra, the seismic unrest lasted more than a year and included
538 numerous $M > 4$ earthquakes, with > 5 m accumulated uplift of the caldera floor since the last
539 eruption in 2005 (Vásconez et al., 2018). Long unrest periods at Sierra Negra, also noted in 2005
540 (Geist et al., 2008), could be related to larger accumulation of magma in the shallow reservoir
541 accommodated thanks to trapdoor faulting (Jónsson et al., 2005) and evidenced by the large-scale
542 ground deformation and large earthquakes prior to its eruptions; such unrest patterns have not yet
543 been observed at other Galápagos volcanoes. It is worth noting that the volume withdrawn from the
544 reservoirs calculated from InSAR during the 2015 Wolf eruption (Xu et al., 2016; Novellis et al.,
545 2017; Stock et al. in review) are about 5 to 10 times smaller than the emitted volume, even when
546 converting the bulk deposit volume into dense rock equivalent. Such discrepancy can be related to
547 the role of the magma compressibility in the reservoir (Rivalta and Segall, 2008) and is consistent
548 with most of the magma deriving directly from a deep magma storage region, as suggested by
549 petrological barometry and the occurrence of syn-eruptive deflation of a deeper reservoir (Stock et
550 al., in review). This process has a direct implication for hazard assessment as it suggests a major
551 disconnect between pre-eruptive ground deformation, which is one of the main monitoring signals
552 for remote Galápagos volcanoes, and the eruptive processes. As Fernandina unrest in 2017 and 2018
553 shared the same deformation characteristics as Wolf unrest in 2015, it is possible that these
554 eruptions share similar pre-eruptive processes.

555

556 **6.2. Eruption dynamics at Wolf volcano**

557 Although reticulite has not been previously described, reports suggest that this may in fact be a
558 common product of recent eruptions in Galápagos (Dennis Geist, pers. Com.). Such scoria are likely
559 to break down easily due to weathering at the surface and so are unlikely to be found unless field
560 work is done soon after an eruption. The occurrence of reticulite scoria during the 2015 Wolf
561 eruption is evidence of the high lava fountaining (Mangan and Cashman, 1996) that was also
562 observed during the Wolf 1982 intra-caldera activity (Schatz and Schatz, 1983; Geist et al., 2005).
563 The reticulite scoria is associated to the high TADR at the beginning of the 2015 eruption. We note
564 that the 1982 and 2015 Wolf eruptions are comparable, in terms of their eruptive style and intensity,
565 to typical Hawaiian eruptions (Houghton and Gonnermann, 2008).

566 The average eruption rates calculated for both studied Wolf eruptions ($14.2\text{-}76.1$ m³/s, dense rock
567 equivalent = bulk*0.75) are similar to previous Galápagos eruptions at Fernandina (1988: 58 m³/s;
568 2009: 27.5 m³/s; 2017: $22.5\text{-}77.7$ m³/s; 2018: $17.4\text{-}51.8$ m³/s), Cerro Azul (1998: 17 m³/s), and
569 Sierra Negra (2018: $14.2\text{-}42.2$ m³/s) but are smaller than the 1979 (130 m³/s) and 2005 (163 m³/s)

570 eruptions at Sierra Negra (Rowland et al., 2003; Geist et al., 2008; Vásconez et al., 2018). Similar
571 eruptive dynamics between Wolf, Cerro Azul and Fernandina could explain their common
572 morphology (Mouginis-Mark et al., 1996). Geist et al. (2005) propose that the unusually steep
573 slopes that make up the upper flank of Wolf edifice are responsible for the dominance of ‘a‘ā lava
574 flow. However, most of the lava fields (flank and caldera) produced during the 1982 and 2015 Wolf
575 eruptions were ‘a‘ā, irrespectively of the slope angle. Pāhoehoe flows were only confirmed on the
576 eastern side of the caldera from the 1982 eruption and on top of the ‘a‘ā deposits close to the
577 circumferential fissure from the 2015 eruption. From MIROVA-derived data and images from the
578 2015 eruption, we infer that these pāhoehoe flows close to the circumferential fissure were
579 emplaced between 04 and 11 June, when TADR were systematically $< 10 \text{ m}^3/\text{s}$ (average $6.5 \text{ m}^3/\text{s}$).
580 In contrast, ‘a‘ā lavas emplaced between 25 and 31 May were characterized by average TADR of
581 $89.8 \text{ m}^3/\text{s}$. Therefore, we propose that the high ‘a‘ā/pāhoehoe area ratio is caused by high eruption
582 rates ($>10 \text{ m}^3/\text{s}$, Rowland and Walker, 1990), and that pāhoehoe at Wolf are mostly associated with
583 the waning phase of the eruptions. Initial activity during the 1982 and 2015 Wolf eruptions, where
584 eruption rates are highest, are associated with significant SO_2 outgassing. This is similar to the 2005
585 eruption of Sierra Negra, but not other western Galapagos eruptions (i.e. at Fernandina and Cerro
586 Azul), where the eruption rates are comparable, suggesting a decoupling between the magma
587 volatile behavior and eruption rate.

588 We note that the 2015 eruption of Wolf volcano is the fourth largest Galapagos eruption since
589 quantitative data are available (i.e. 1979), only behind Sierra Negra eruptions (1979, 2005, 2018;
590 Vásconez et al., 2018). This might be due to the long quiescence at Wolf between the 1982 and the
591 2015 eruptions (33 years), which is significantly greater than typical quiescence at other active
592 volcanoes in the western archipelago (e.g. Fernandina and Cerro Azul). Lastly, the 1982 and 2015
593 Wolf eruptions evolved from multiple vents, which appears to be common during moderate to large
594 eruptions in the Galápagos (Sierra Negra 1979, 2005 and 2018; Fernandina 1995, Cerro Azul 1998).
595 It is important to document and study such behavior in detail, as it has a direct impact on the area
596 potentially at risk during eruptions.

597

598 **7. Conclusions**

599 Despite the remoteness of Wolf volcano, we demonstrate how eruption chronology can be
600 reconstructed using a combination of ground-based geophysical surveillance, eyewitness accounts,
601 remote sensing data, and post eruptive fieldwork. The 1982 and 2015 eruptions at Wolf volcano are
602 characterized by a rapid, intense initial phase and multiple eruptive vents (SE radial fissure and
603 caldera vent for the 1982 eruption; SE to E circumferential fissure and caldera vent for the 2015
604 eruption). Both eruptions showed a high lava fountaining phase, which was associated with high

605 eruption rates and intense outgassing. We report the first detected Galápagos cryptotephra to reach
606 continental Ecuador, which was associated with the high fountaining event in 2015. This material
607 was transported 1400 km away from its source within a 15 km-high gas plume, carried east by
608 stratospheric winds. The main products of the 1982 and 2015 eruptions of Wolf were large ‘a‘ā lava
609 fields, with pāhoehoe deposits exclusively associated with the waning phase of the eruptions. The
610 2015 eruption was larger than the 1982 eruption and represents the fourth largest eruption in
611 Galápagos over the last 40 years. Our new reconstruction of the chronology and phenomenology of
612 the 1982 and 2015 Wolf eruptions provides some of the most detailed constraints on the eruptive
613 dynamics at western Galápagos shield volcanoes to date, which is essential for volcanic
614 surveillance, hazard assessment and contingency planning in one of the most ecologically valuable
615 locations on Earth.

616

617 **Acknowledgments**

618 We acknowledge the logistical support of the Charles Darwin Research Station and permission of
619 the Galápagos National Park Service, without whom this work could not have been accomplished,
620 in particular park ranger Wilson Villamar for his assistance on the field. We also thank captain
621 Lenin Cruz and its crew for their enthusiasm and crucial help sailing to Wolf volcano. Antonio
622 Proaño and Francisco Vásquez (IG-EPN) help during fieldwork is also acknowledged. BB thanks
623 the project Strengthening Resilience in Volcanic Areas (STREVA) that provided the UAV for the
624 photogrammetric projects. BB and PR acknowledge the Secretaría de Gestión de Riesgos,
625 Galápagos, and the Ecuadorian Navy for their logistical support with helicopter overflights. MJS
626 acknowledges support from a Charles Darwin and Galapagos Islands Junior Research Fellowship at
627 Christ’s College, Cambridge. MG was supported by a NERC studentship (NE/L002507/1). MB was
628 supported the NERC Centre for the Observation and Modelling of Earthquakes, Volcanoes and
629 Tectonics (COMET) and by an appointment to the NASA Postdoctoral Program at the Jet
630 Propulsion Laboratory, administered by the Universities Space and Research Association (USRA)
631 through a contract with NASA. Sentinel-1 images were derived from Copernicus SAR data
632 obtained at <https://schihub.copernicus.eu>. Additional funding for fieldwork was provided by the
633 Jeremy Willson Charitable Trust and the Mineralogical Society of Great Britain and Ireland.

634

635 **References**

636 Bagnardi, M (2014) Dynamics of Magma Supply, Storage and Migration at Basaltic Volcanoes:
637 Geophysical Studies of the Galápagos and Hawaiian Volcanoes. Open Access Dissertations. 1179.
638 https://scholarlyrepository.miami.edu/oa_dissertations/1179

639 Belousov A, Belousova M (2018) Dynamics and viscosity of ‘a’a and pahoehoe lava flows of the
640 2012–2013 eruption of Tolbachik volcano, Kamchatka (Russia). *Bulletin of Volcanology* 80:6 . doi:
641 10.1007/s00445-017-1180-2

642 Bernard B (2013) Homemade ashmeter: a low-cost, high-efficiency solution to improve tephra
643 field-data collection for contemporary explosive eruptions. *Journal of Applied Volcanology* 2:1 .
644 doi: [10.1186/2191-5040-2-1](https://doi.org/10.1186/2191-5040-2-1)

645 Bernard B, Ramon P, Wright HM, Guevara A, Hidalgo S, Pacheco DA, Narváez D, Vásconez F
646 (2015) Preliminary Results on the 2015 Eruption of Wolf Volcano, Isabela Island, Galápagos:
647 Chronology, Dispersion of the Volcanic Products, and Insight into the Eruptive Dynamics. In:
648 Abstract volume of the 2015 AGU Fall Meeting. San Francisco – USA

649 Chadwick WW, Howard KA (1991) The pattern of circumferential and radial eruptive fissures on
650 the volcanoes of Fernandina and Isabela islands, Galapagos. *Bulletin of Volcanology* 53:259–275

651 Chevrel MO, Platz T, Hauber E, Baratoux D, Lavallée Y, Dingwell DB (2013) Lava flow rheology:
652 A comparison of morphological and petrological methods. *Earth and Planetary Science Letters*
653 384:109–120 . doi: 10.1016/j.epsl.2013.09.022

654 Coppola D, Laiolo M, Cigolini C, Donne DD, Ripepe M (2016) Enhanced volcanic hot-spot
655 detection using MODIS IR data: results from the MIROVA system. *Geological Society, London,*
656 *Special Publications* 426:181–205 . doi: 10.1144/SP426.5

657 Coppola D, Laiolo M, Piscopo D, Cigolini C (2013) Rheological control on the radiant density of
658 active lava flows and domes. *Journal of Volcanology and Geothermal Research* 249:39–48 . doi:
659 10.1016/j.jvolgeores.2012.09.005

660 De Novellis V, Castaldo R, De Luca C, Pepe S, Zinno I, Casu F, Lanari R, Solaro G (2017) Source
661 modelling of the 2015 Wolf volcano (Galápagos) eruption inferred from Sentinel 1-A DInSAR
662 deformation maps and pre-eruptive ENVISAT time series. *Journal of Volcanology and Geothermal*
663 *Research* 344:246–256 . doi: 10.1016/j.jvolgeores.2017.05.013

664 Dietterich HR, Poland MP, Schmidt DA, Cashman KV, Sherrod DR, Espinosa AT (2012) Tracking
665 lava flow emplacement on the east rift zone of Kīlauea, Hawai‘i, with synthetic aperture radar
666 coherence. *Geochemistry, Geophysics, Geosystems* 13: . doi: 10.1029/2011GC004016

667 Geist DJ, Harpp KS, Naumann TR, Poland M, Chadwick WW, Hall M, Rader E (2008) The 2005
668 eruption of Sierra Negra volcano, Galápagos, Ecuador. *Bulletin of Volcanology* 70:655–673 . doi:
669 10.1007/s00445-007-0160-3

670 Geist DJ, Naumann TR, Standish JJ, Kurz MD, Harpp KS, White WM, Fornari DJ (2005) Wolf
671 Volcano, Galápagos Archipelago: Melting and Magmatic Evolution at the Margins of a Mantle
672 Plume. *J Petrology* 46:2197–2224. doi: 10.1093/petrology/egi052

673 Giordano D, Russell JK, & Dingwell DB (2008) Viscosity of Magmatic Liquids: A Model. *Earth &*
674 *Planetary Science Letters*, 271, 123-134

675 Global Volcanism Program, 2013. Wolf (353020) *in* *Volcanoes of the World*, v. 4.7.4. Venzke, E
676 (ed.). Smithsonian Institution. Downloaded 30 Sep 2018 ([http://volcano.si.edu/volcano.cfm?](http://volcano.si.edu/volcano.cfm?vn=353020)
677 [vn=353020](http://volcano.si.edu/volcano.cfm?vn=353020)). <https://doi.org/10.5479/si.GVP.VOTW4-2013>

678 González J, Montes C, Rodríguez J, Tapia W (2008) Rethinking the Galapagos Islands as a
679 Complex Social-Ecological System: Implications for Conservation and Management. *Ecology and*
680 *Society* 13: . doi: 10.5751/ES-02557-130213

681 Houghton BF, Gonnermann HM (2008) Basaltic explosive volcanism: Constraints from deposits
682 and models. *Chemie der Erde - Geochemistry* 68:117–140 . doi: 10.1016/j.chemer.2008.04.002

683 Hulme G (1974) The interpretation of lava flow morphology. *Geophysical Journal of the Royal*
684 *Astronomy Society* 39:361–383

685 Jeffreys H (1925) The flow of water in an inclined channel of rectangular section. *Philos. Mag. Ser.*
686 *6* 49 (293), 793–807

687 Jónsson S, Zebker H, Amelung F (2005) On trapdoor faulting at Sierra Negra volcano, Galápagos.
688 *Journal of Volcanology and Geothermal Research* 144:59–71 . doi:
689 10.1016/j.jvolgeores.2004.11.029

690 Kurz MD, Geist D (1999) Dynamics of the Galapagos hotspot from helium isotope geochemistry.
691 *Geochimica et Cosmochimica Acta* 63:4139–4156 . doi: 10.1016/S0016-7037(99)00314-2

692 Lange R, Carmichael I (1990) Hydrous basaltic andesites associated with minette and related lavas
693 in Western Mexico. *Journal of Petrology* 31:1225–1259

694 Mangan MT, Cashman KV (1996) The structure of basaltic scoria and reticulite and inferences for
695 vesiculation, foam formation, and fragmentation in lava fountains. *Journal of Volcanology and*
696 *Geothermal Research* 73:1–18

697 McCormick BT, Herzog M, Yang J, Edmonds M, Mather TA, Carn SA, Hidalgo S, Langmann B
698 (2014) A comparison of satellite-and ground-based measurements of SO₂ emissions from
699 Tungurahua volcano, Ecuador. *Journal of Geophysical Research: Atmospheres* 119:4264–4285 .
700 doi: 10.1002/2013JD019771

701 Mougini-Mark PJ, Rowland SK, Garbeil H (1996) Slopes of Western Galapagos volcanoes from
702 airborne interferometric radar. *Geophys Res Lett* 23:3767–3770 . doi: 10.1029/96GL03280

703 Munro DC, Rowland SK (1996) Caldera morphology in the western Galápagos and implications for
704 volcano eruptive behavior and mechanisms of caldera formation. *Journal of Volcanology and*
705 *Geothermal Research* 72:85–100. doi: 10.1016/0377-0273(95)00076-3

706 Naumann T, Geist D (2000) Physical volcanology and structural development of Cerro Azul
707 Volcano, Isabela Island, Galápagos: implications for the development of Galápagos-type shield
708 volcanoes. *Bulletin of Volcanology* 61:497–514. doi: 10.1007/s004450050001

709 Nichols RL (1939) Viscosity of lava. *J. Geol.* 47, 290–302.

710 Reynolds RW, Geist D, Kurz MD (1995) Physical volcanology and structural development of Sierra
711 Negra volcano, Isabela Island, Galápagos archipelago. *Geological Society of America Bulletin*
712 107:1398–1410. doi: 10.1130/0016-7606(1995)107<1398:PVASDO>2.3.CO;2

713 Rivalta E, Segall P (2008) Magma compressibility and the missing source for some dike intrusions.
714 *Geophysical Research Letters* 35: . doi: 10.1029/2007GL032521

715 Rowe C.A, Aster RC, Borchers B, Young CJ (2002). An automatic, adaptive algorithm for refining
716 phase picks in large seismic data sets. *Bulletin of the Seismological Society of America* 92, no. 5,
717 1660–1674, doi: 10.1785/0120010224.

718 Rowland SK, Harris AJL, Wooster MJ, Amelung F, Garbeil H, Wilson L, Mouginiis-Mark PJ (2003)
719 Volumetric characteristics of lava flows from interferometric radar and multispectral satellite data:
720 the 1995 Fernandina and 1998 Cerro Azul eruptions in the western Galápagos. *Bulletin of*
721 *Volcanology* 65:311–330

722 Rowland SK, Walker GP (1990) Pahoehoe and aa in Hawaii: volumetric flow rate controls the lava
723 structure. *Bulletin of Volcanology* 52:615–628

724 Ryan, W.B.F., S.M. Carbotte, J.O. Coplan, S. O'Hara, A. Melkonian, R. Arko, R.A. Weissel, V.
725 Ferrini, A. Goodwillie, F. Nitsche, J. Bonczkowski, and R. Zemsky (2009), Global Multi-Resolution
726 Topography synthesis, *Geochem. Geophys. Geosyst.*, 10, Q03014, doi: 10.1029/2008GC002332

727 Schatz H, Schatz I The eruption of the volcano Wolf (Albemarle, Galápagos islands, Ecuador) in
728 1982—Report of eye-witnesses [in German]. *Ber Nat-med Verein Innsbruck* 70:17–28

729 Simkin T (1984) Geology of Galapagos. *Biol J Linn Soc* 21:61–75. doi: 10.1111/j.1095-
730 8312.1984.tb02053.x

731 Simkin T, Howard K (1970) Caldera collapse in the Galapagos islands. *Science* 169:429–437

732 Vasconez FJ, Ramón P, Hernandez S, Hidalgo S, Bernard B, Ruiz M, Alvarado A, Femina PL, Ruiz
733 G (2018) The different characteristics of the recent eruptions of Fernandina and Sierra Negra
734 volcanoes (Galápagos, Ecuador). *J* 11:127–133

735 Withers M, Aster R, Young C, Beiriger J, Harris M, Moore S, Trujillo J (1998) A comparison of
736 select trigger algorithms for automated global seismic phase and event detection. *Bulletin of the*
737 *Seismological Society of America* ; 88 (1): 95–106.

738 Xu W, Jónsson S, Ruch J, Aoki Y (2016) The 2015 Wolf volcano (Galápagos) eruption studied
739 using Sentinel-1 and ALOS-2 data. Research Letter. doi: 10.1002/2016GL069820